Supporting Information

Structure and electrochemical properties of carbon nanostructures derived from nickel (II) and iron (II) phthalocyanines

Angela Sanchez-Sanchez[a,*], *Maria Teresa Izquierdo*[b], *Sandrine Mathieu*[c], *Jaafar Ghanbaja*[c], *Alain Celzard*[a,*] *and Vanessa Fierro*[a]

[a] Université de Lorraine, CNRS, IJL, F-88000 Epinal, France.

[b] Instituto de Carboquimica, ICB-CSIC, Miguel Luesma Castan, 4, 50018 Zaragoza, Spain.

[c] Université de Lorraine, CNRS, IJL, F-54000 Nancy, France.

E-mail: *A. Sanchez-Sanchez. E-mail: angela.sanchez-sanchez@univ-lorraine.fr. *Alain Celzard: alain.celzard@univ-lorraine.fr

Keywords: metal phthalocyanines, hydrothermal carbonization, catalytic graphitization, supercapacitors.

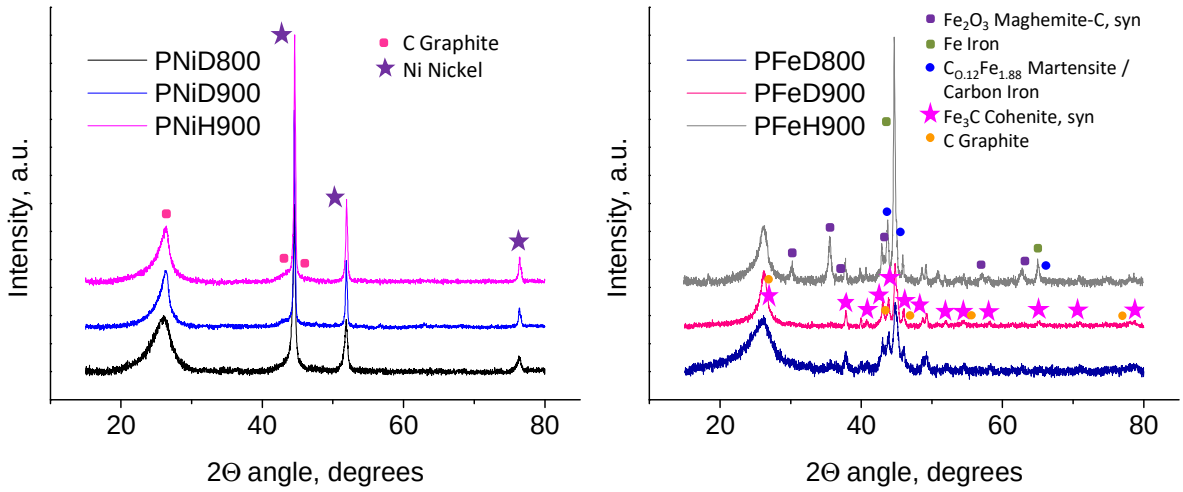

Figure S1. X-ray diffraction patterns of the studied carbons: (a) PNi series; (b) PFe series.

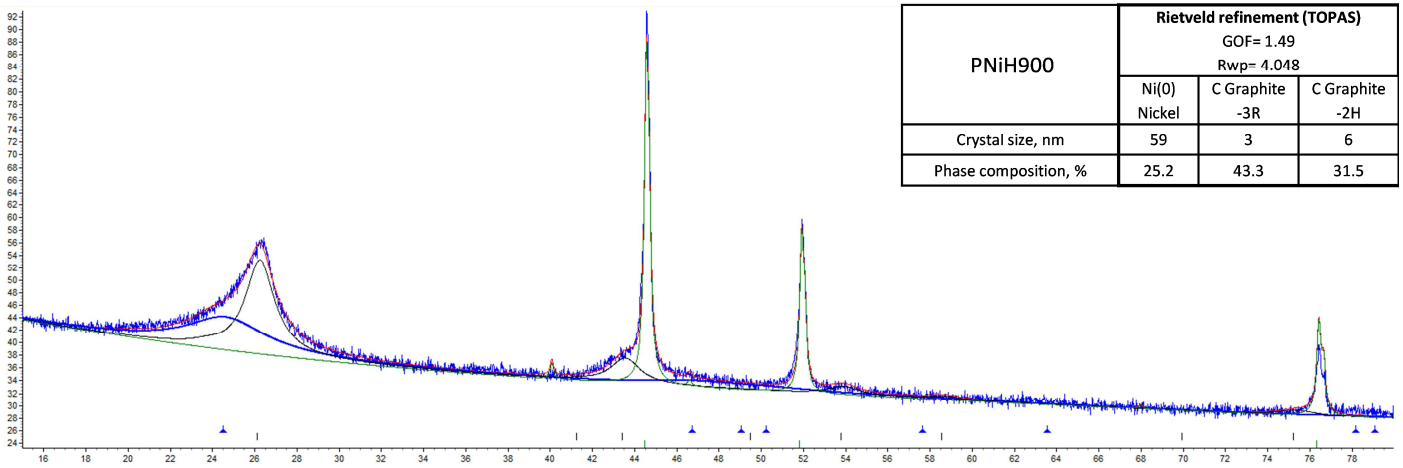

PNiH900	Rietveld refinement (TOPAS) GOF= 1.49 Rwp= 4.048		
	Ni(0) Nickel	C Graphite -3R	C Graphite -2H
Crystal size, nm	59	3	6
Phase composition, %	25.2	43.3	31.5

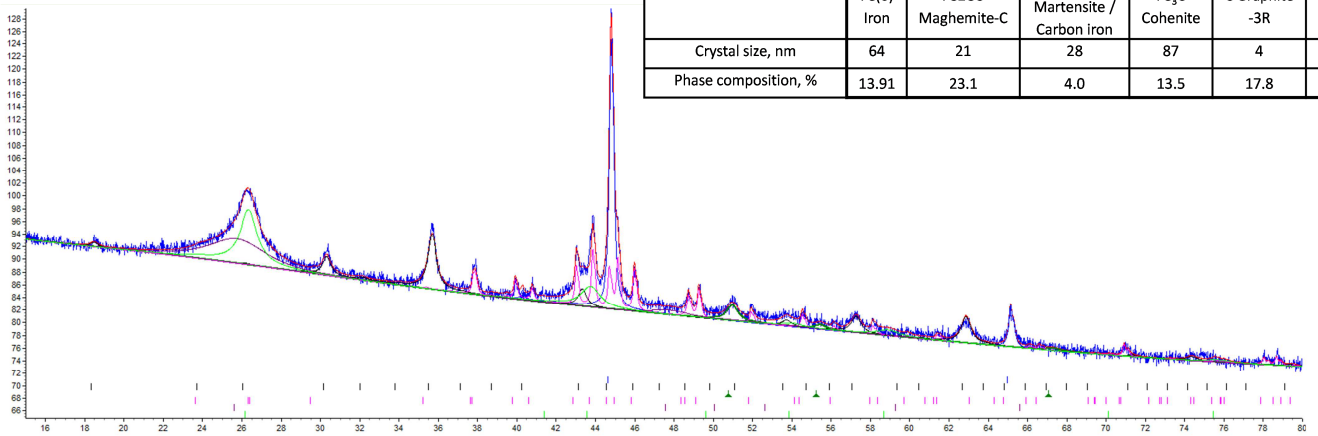

PFeH900	Rietveld refinement (TOPAS) GOF= 1.18 Rwp= 1.394					
	Fe(0) Iron	Fe2O3 Maghemite-C	$C_{0.12}Fe_{1.88}$ Martensite / Carbon iron	Fe_3C Cohenite	C Graphite -3R	C Graphite -2H
Crystal size, nm	64	21	28	87	4	11
Phase composition, %	13.91	23.1	4.0	13.5	17.8	27.7

Figure S2. Quantification of the crystal phases in PNiH900 and PFeH900 materials through Rietveld's refinement (TOPAS software) of their XRD patterns.

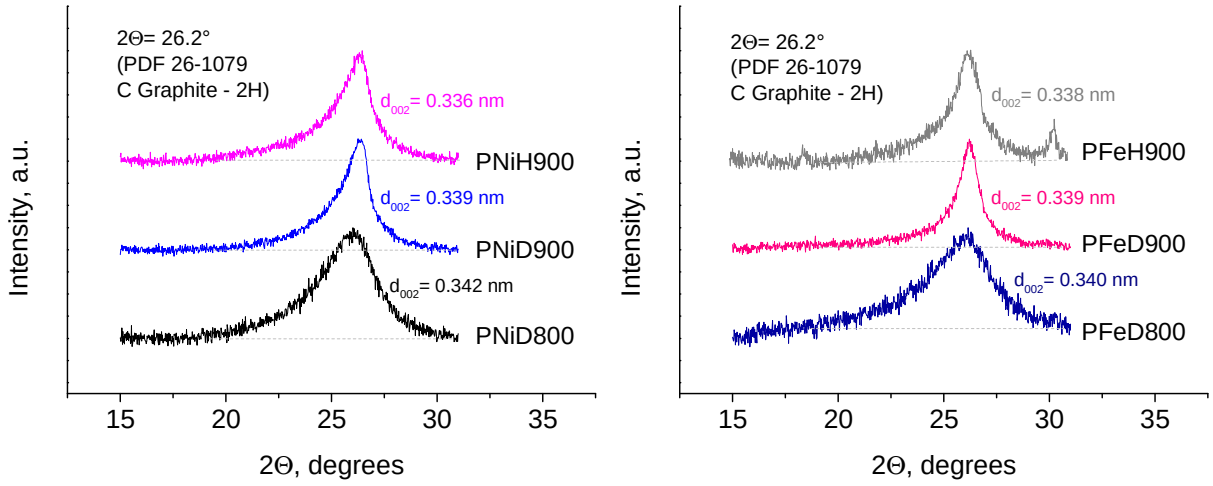

Figure S3. Details of the XRD patterns showing the d_{002} band centred at around 2θ = 26.2° and assigned to graphitic carbon.

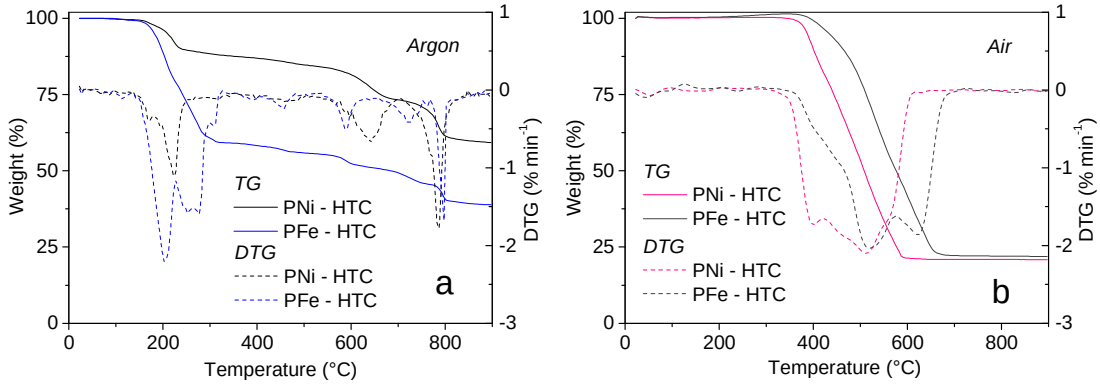

Figure S4. TG and DTG curves of the phthalocyanine-derived materials after HTC: (a) in argon flow; and (b) in air flow.

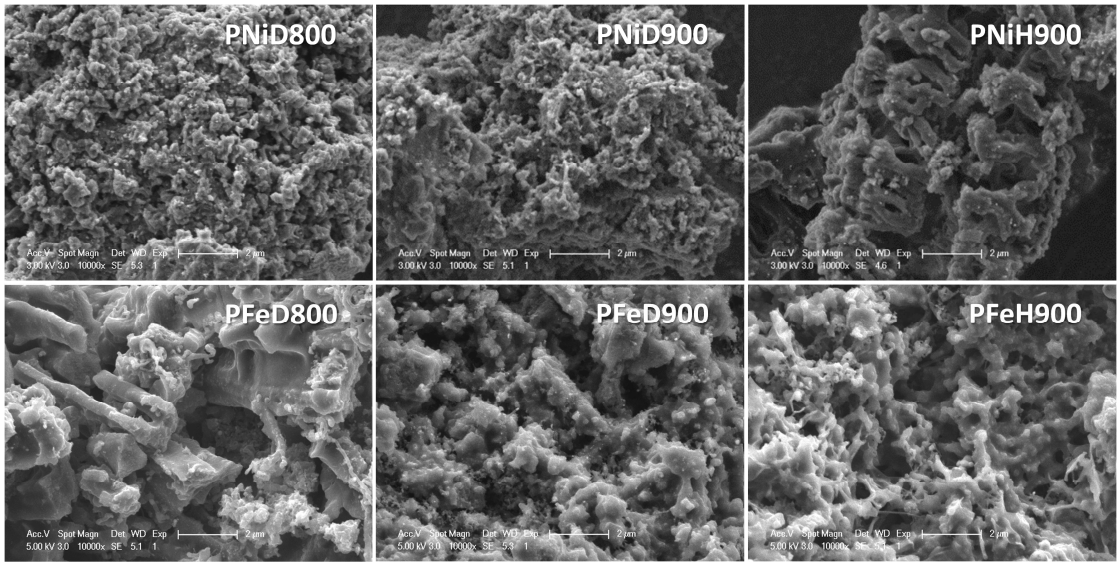

Figure S5. SEM pictures of the studied carbon materials.

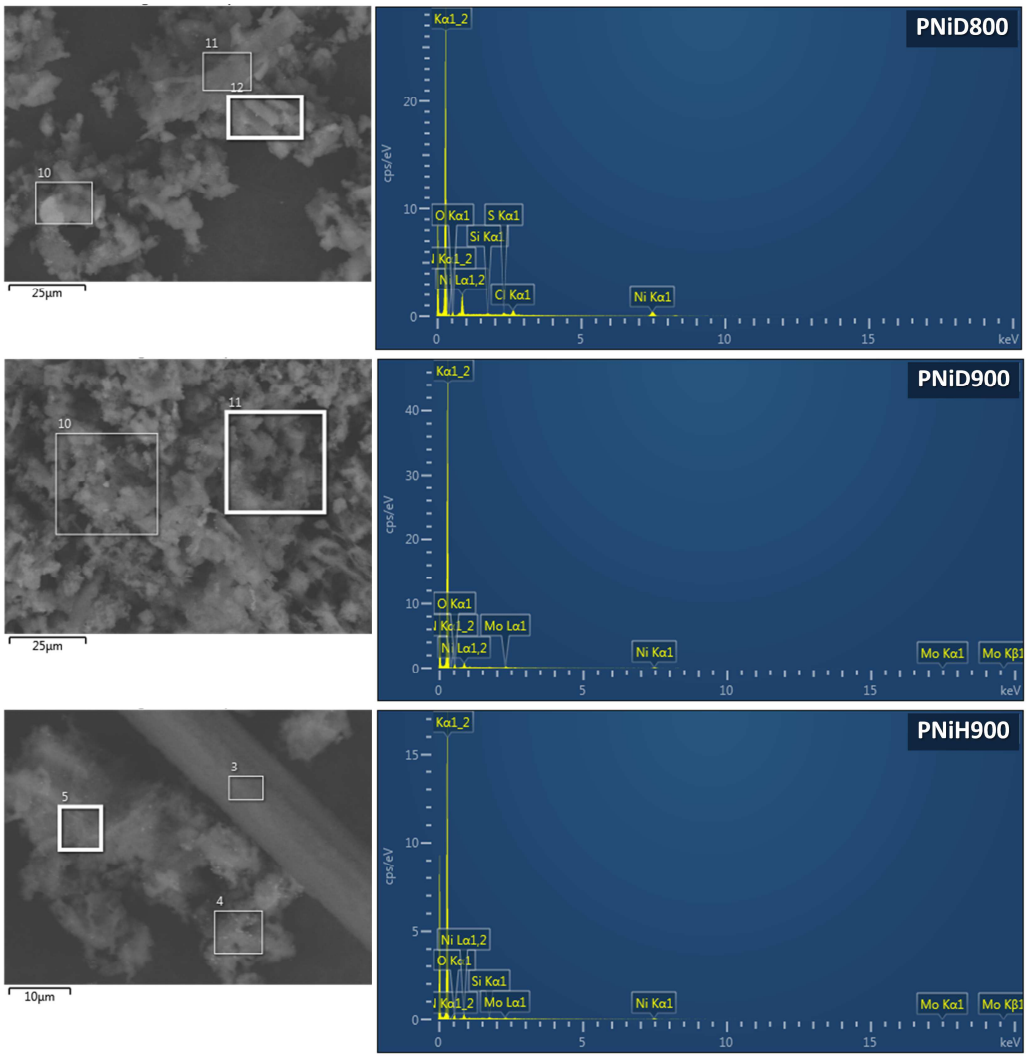

Figure S6. Chemical composition of the PNi–series carbons determined by SEM-EDX.

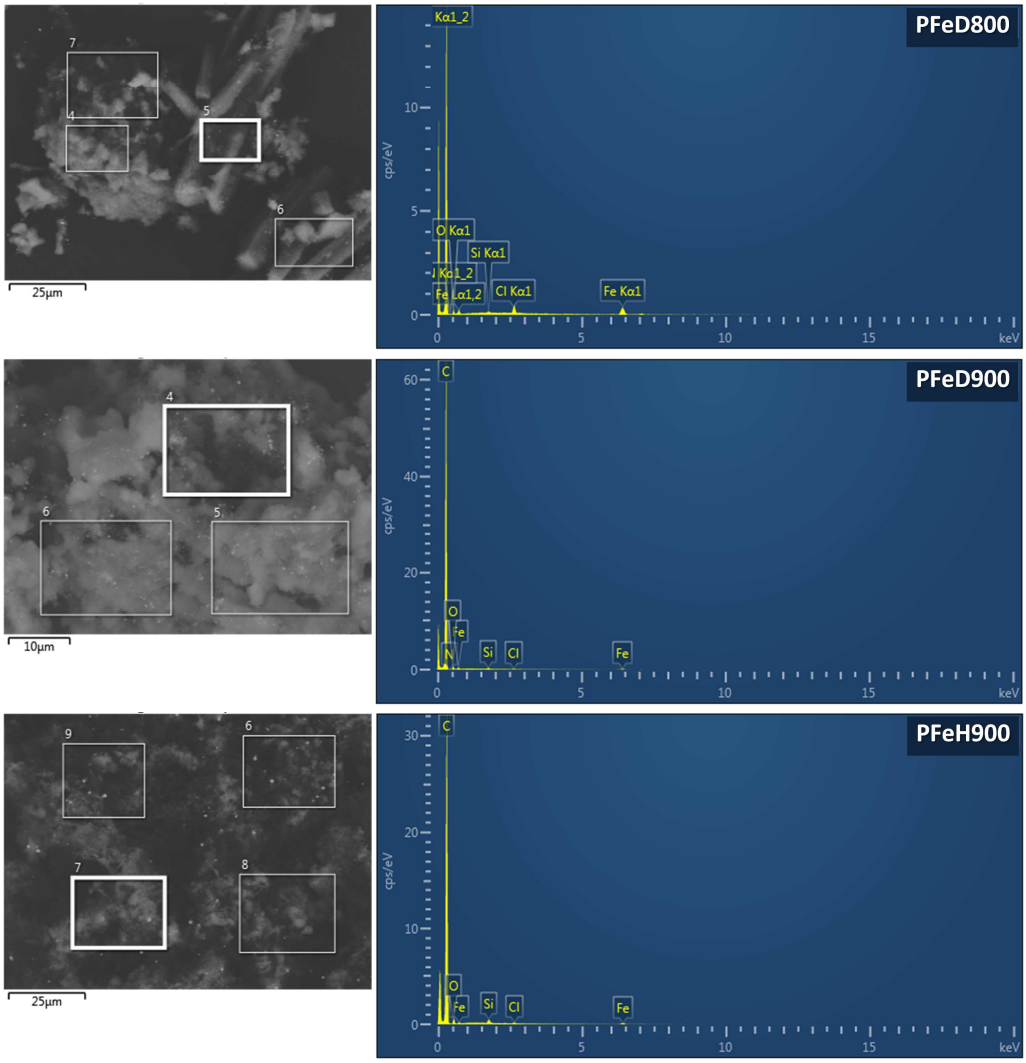

Figure S7. Chemical composition of the PFe–series carbons determined by SEM-EDX.

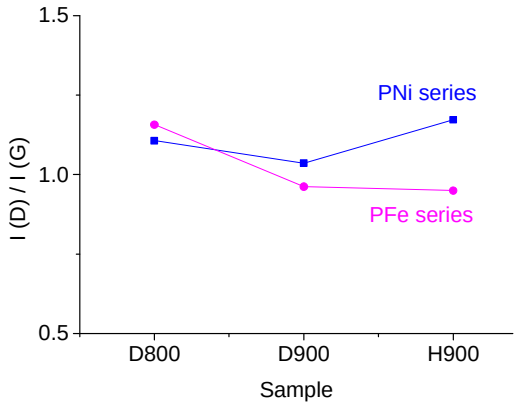

Sample	I(D) (counts)	I(G) (counts)	I(D) / I(G)
PNiD800	1795.9	1622.8	1.11
PNiD900	1572.2	1517.8	1.03
PNiH900	1624.5	1386.0	1.17
PFeD800	2373.9	2052.0	1.16
PFeD900	2143.6	2228.7	0.96
PFeH900	3144.7	3311.7	0.95

Figure S8. Intensities of the D and G bands (left) and intensity ratios, *I*(D) / *I*(G) (right), obtained from the first-order Raman spectra of the carbons.

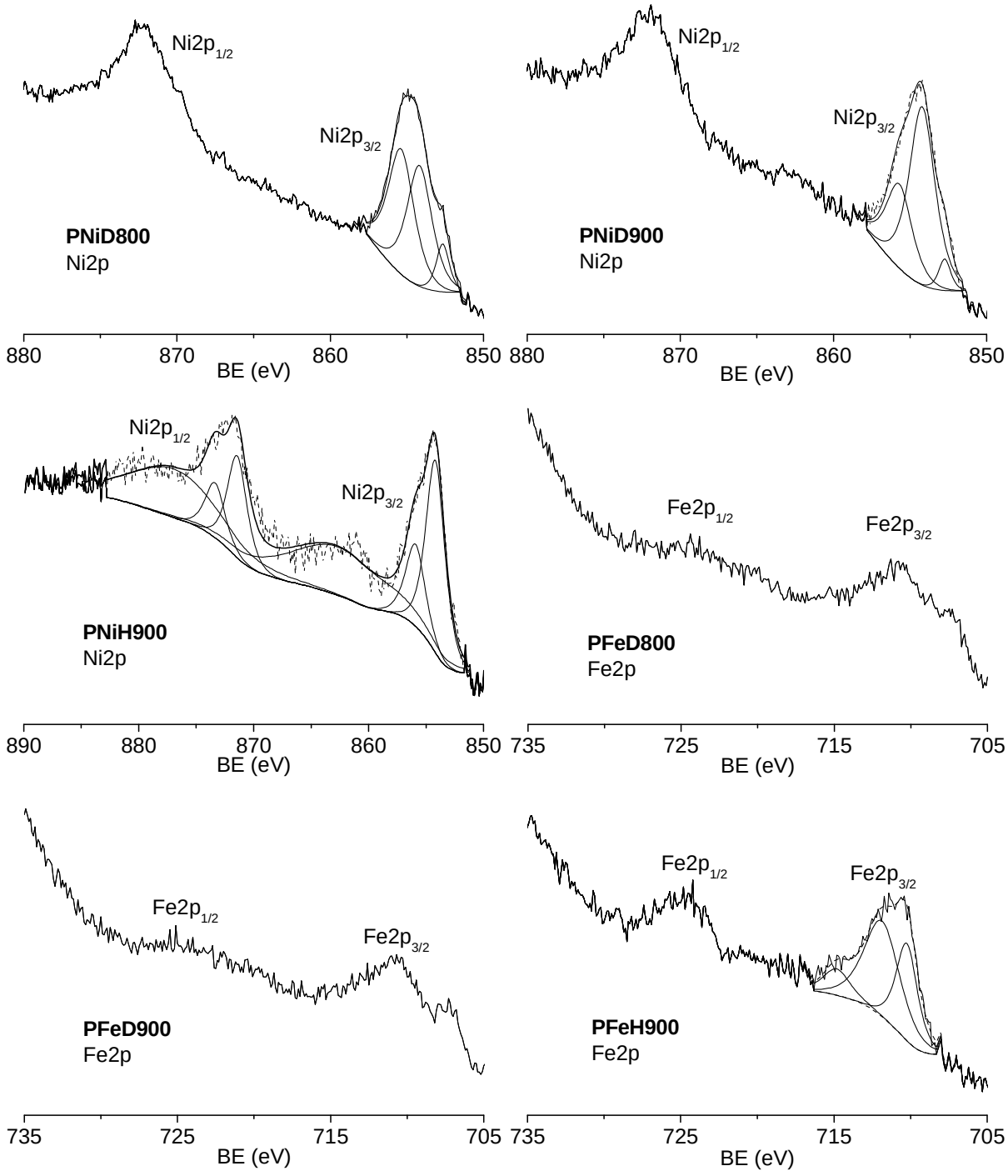

Figure S9. Ni2p and Fe2p high-resolution XPS spectra of the materials.

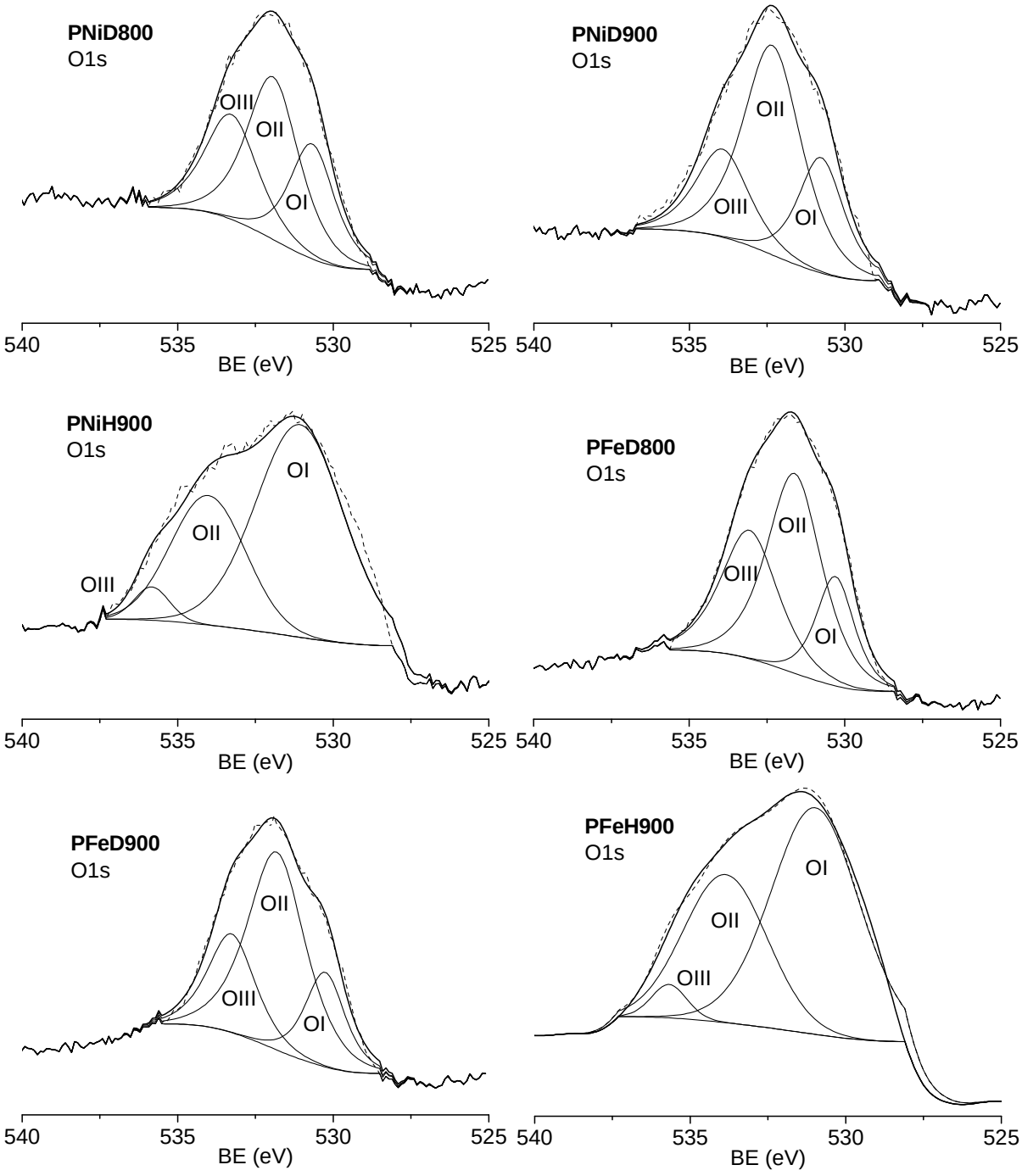

Figure S10. O1s high-resolution XPS spectra of the materials.

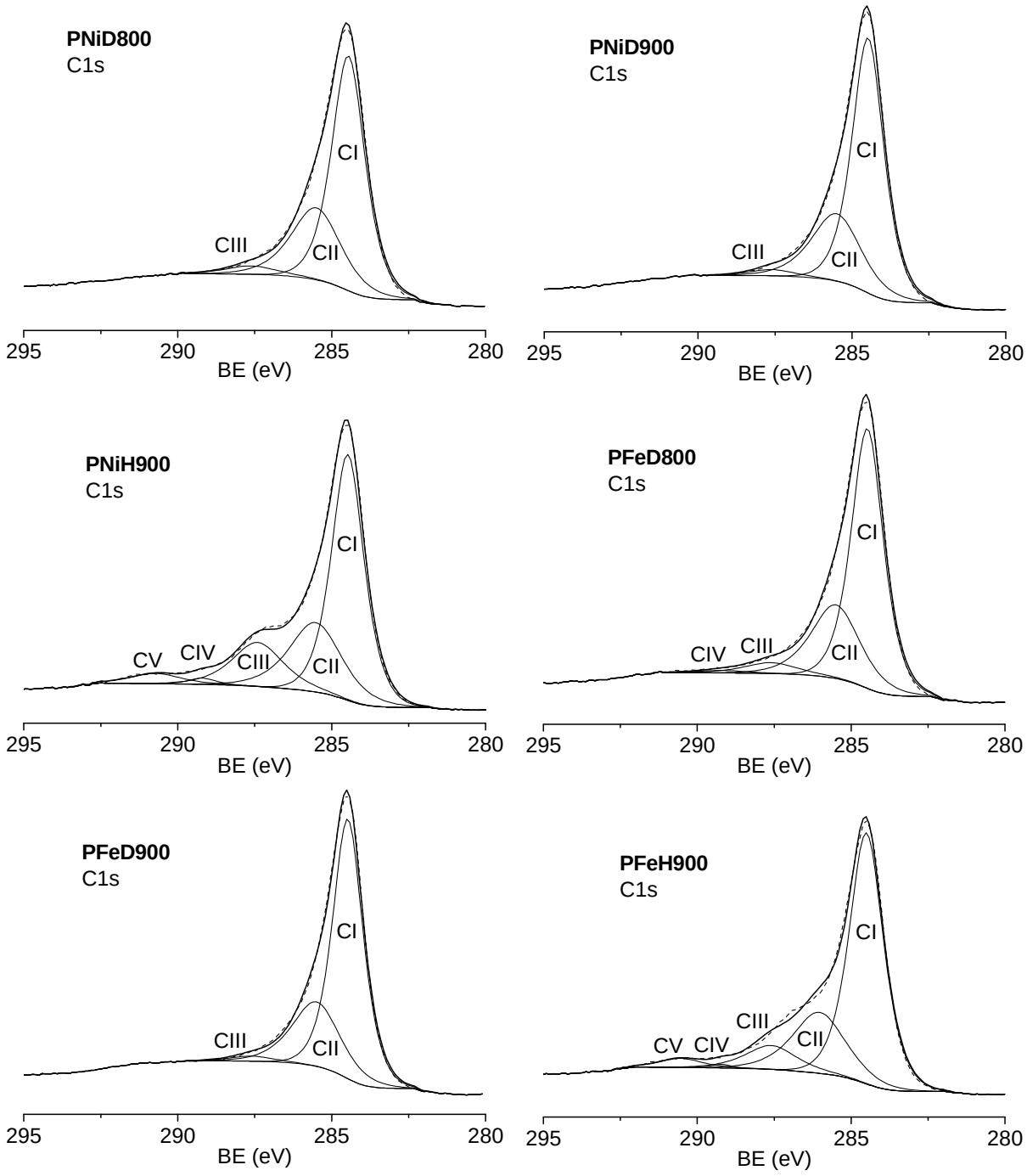

Figure S11. C1s high-resolution XPS spectra of the materials.

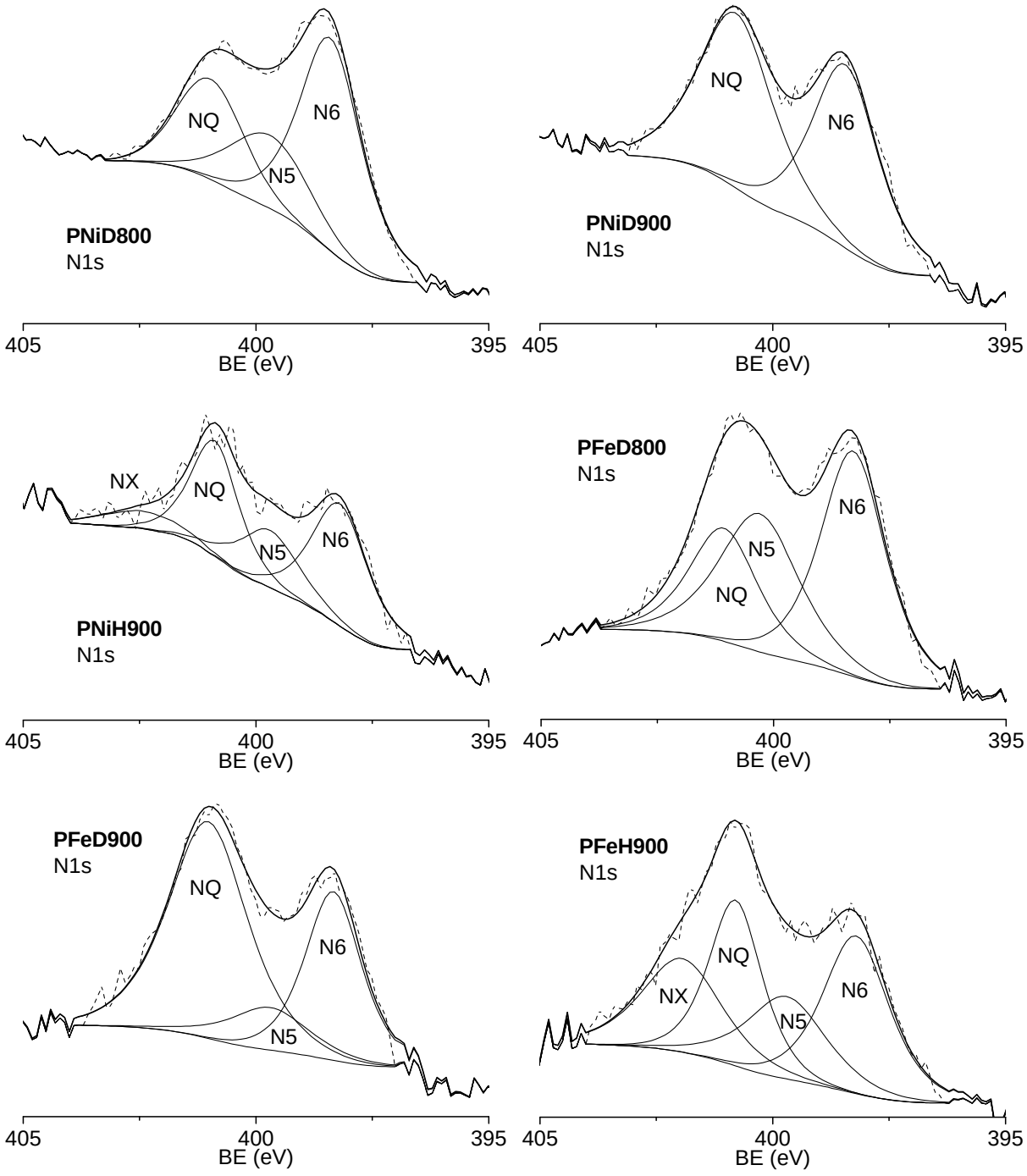

Figure S12. N1s high-resolution XPS spectra of the materials.

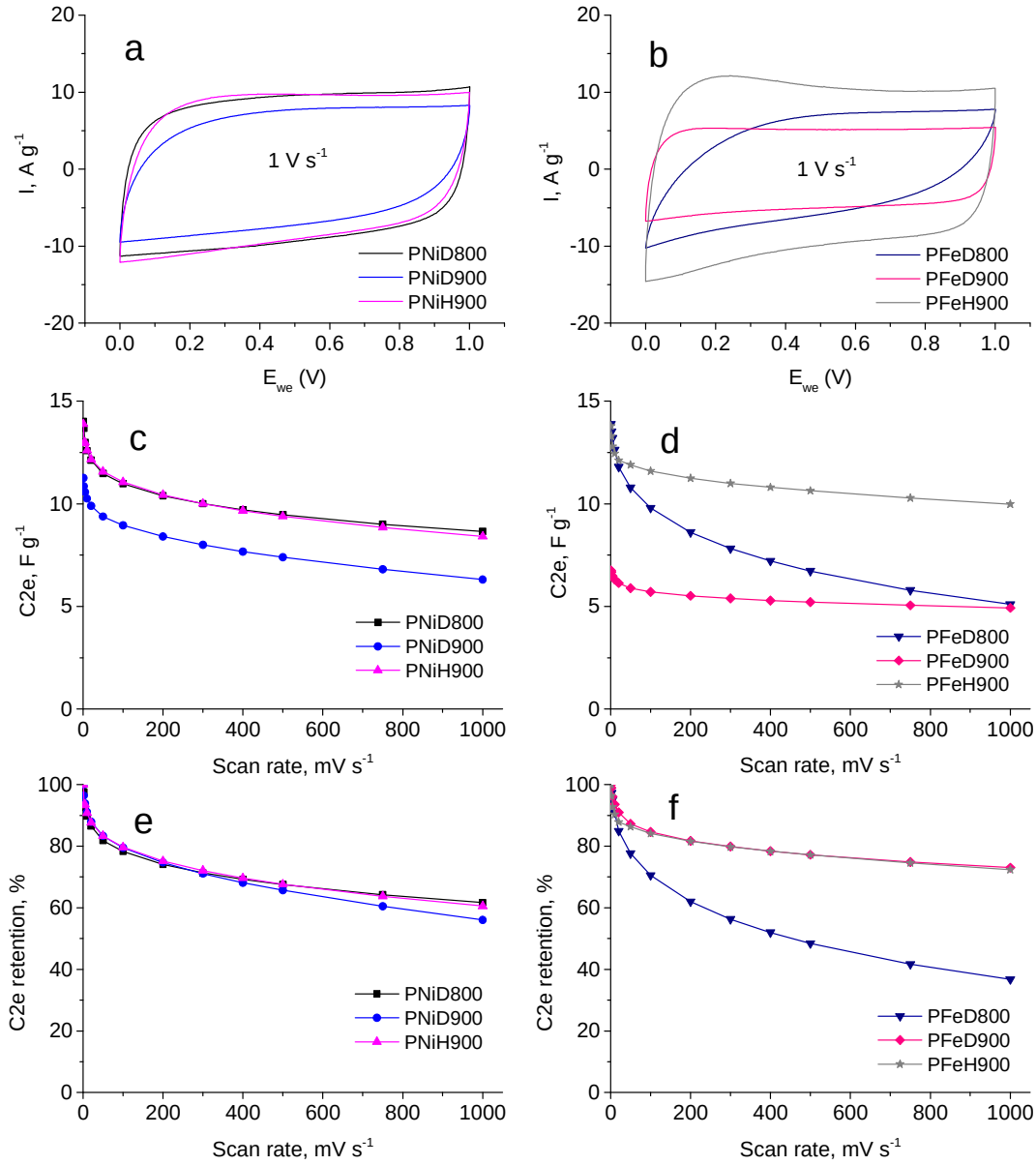

Figure S13. (a,b) Cyclic voltammetry results obtained with a two-electrode cell in 2 mol L^{-1} H_2SO_4 electrolyte within the potential window of 0–1V at a scan rate of 1 V s^{-1}; (c,d) Specific capacitance values at scan rates ranging from 1 mV s^{-1} to 1 V s^{-1}; (e,f) Capacitance retentions from 1 mV s^{-1} to 1 V s^{-1}.

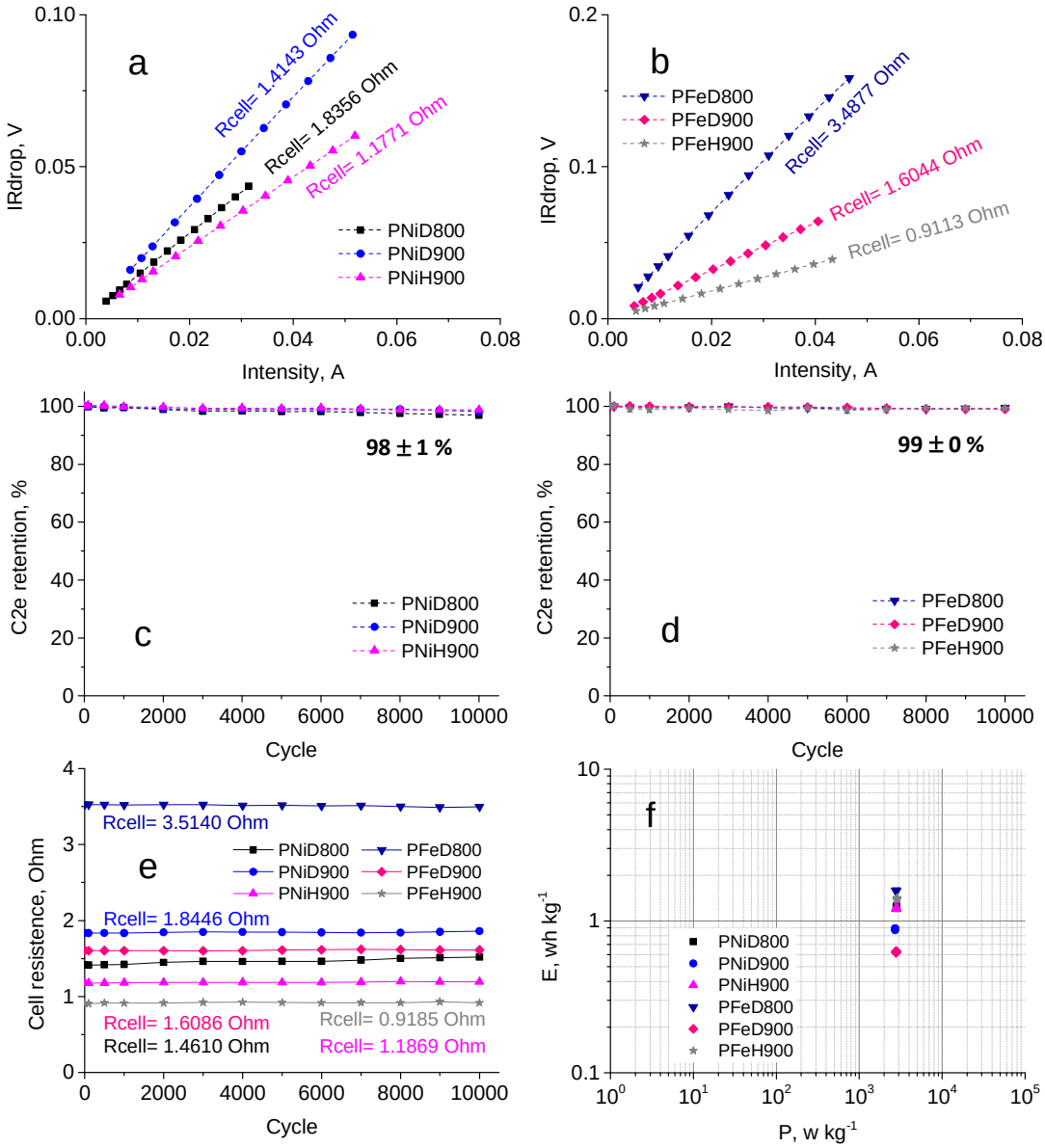

Figure S14. (a,b) Evolution of the ohmic drop, *IR* drop, of the cells with the applied intensity, and calculated cell resistance, R_{cell}; (c,d) Cyclability of the cells measured at the intensity of 5 A g^{-1} up to 10 000 charge-discharge cycles; (e) Evolution of the cell resistance with the number of charge-discharge cycles at the intensity of 5 A g^{-1}. The average resistance of the respective cells is given near each trend line; (f) Evolution of energy and power densities throughout 10 000 charge-discharge cycles, applying a current density of 5 A g^{-1}.

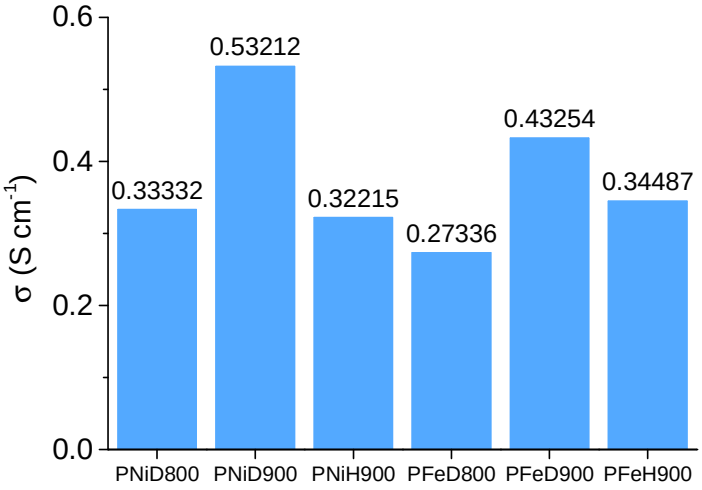

Figure S15. Electrical conductivity of the carbon electrodes.

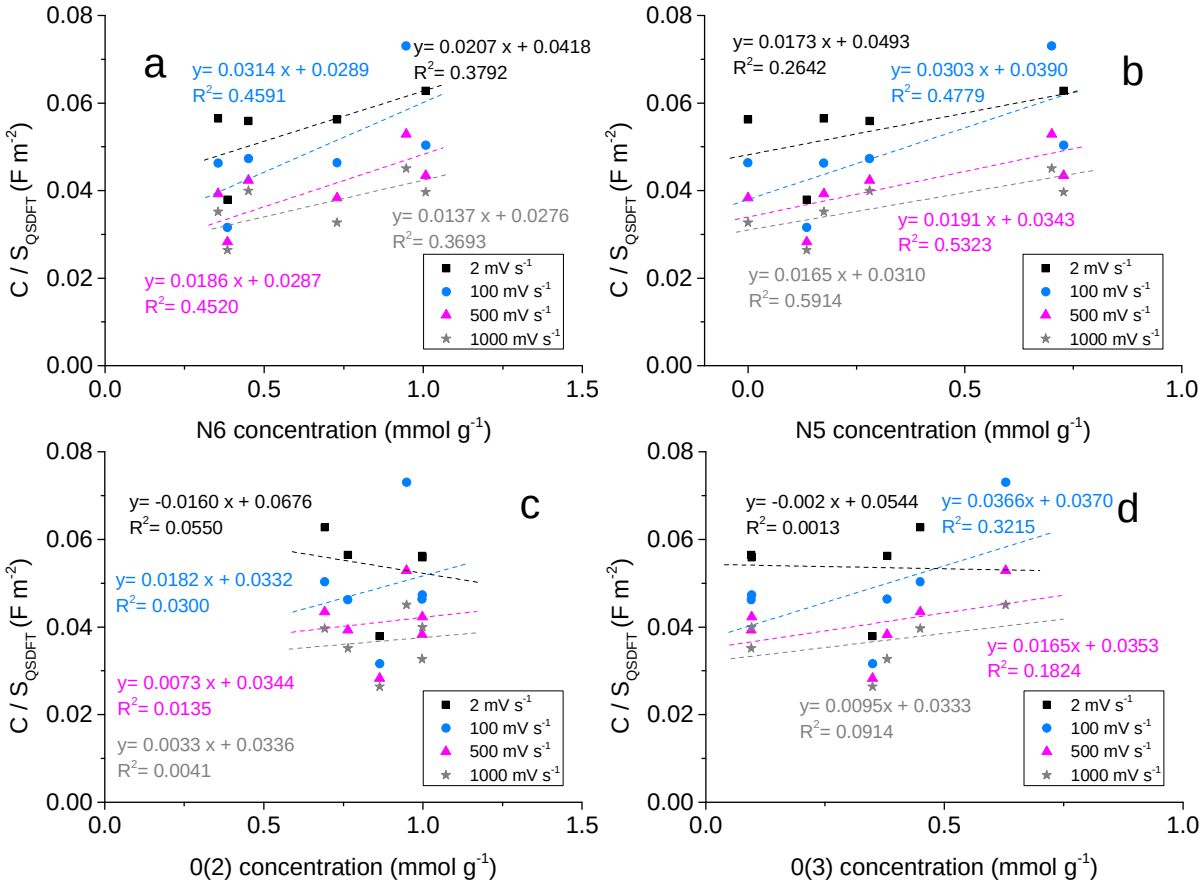

Figure S16. Interfacial capacitance, C/S_{QSDFT}, obtained from CV curves at scan rates between 1 and 1000 mV s^{-1} versus surface concentration of: (a) pyridinic nitrogen; (b) pyrrolic nitrogen; (c) carbonyls, quinones and carboxylic acids; and (d) phenols, ethers, esters and anhydrides.

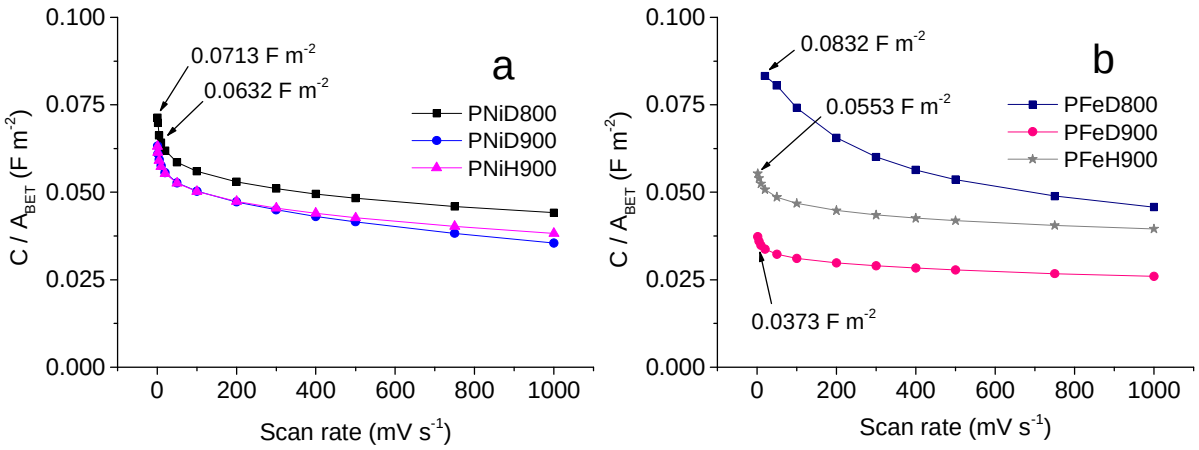

Figure S17. Interfacial capacitance, C/A_{BET}, of the carbon electrodes: (a) PNi series carbons; (b) PFe series carbons.

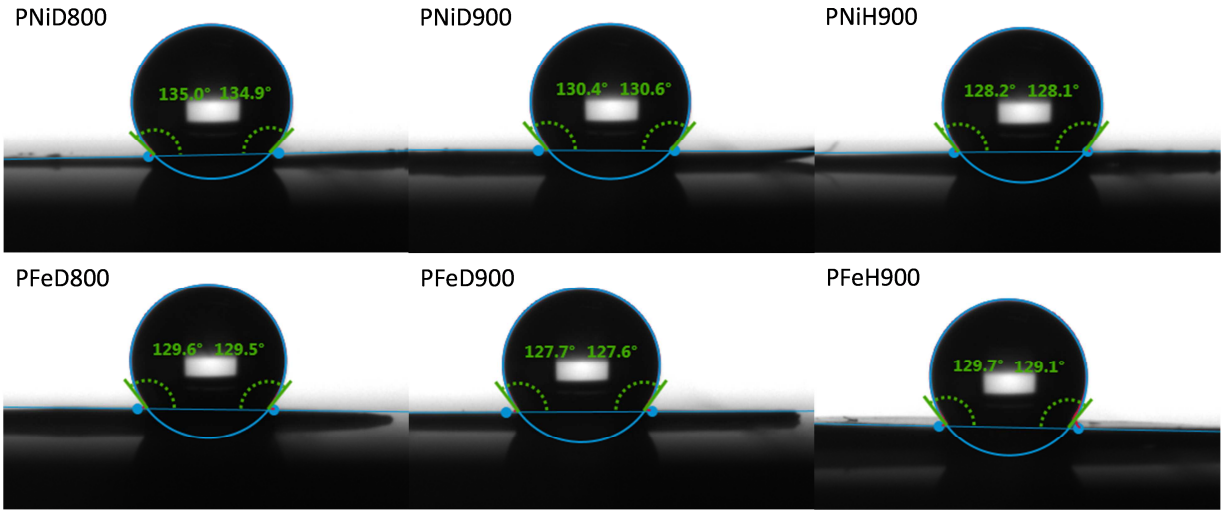

Figure S18. Initial contact angle of 2 mol L^{-1} H_2SO_4 with the carbon electrodes.

Table S1. Surface chemical composition obtained by XPS and contributions to the peaks obtained from the high-resolution spectra of the materials.*

Sample	XPS [at.%]					C1s					O1s			N1s				$Ni2p^{3/2}$				$Fe2p^{3/2}$		
	C	N	O	Ni	Fe	CI BE [eV] A [%]	CII BE [eV] A [%]	CIII BE [eV] A [%]	CIV BE [eV] A [%]	CIV BE [eV] A [%]	O(1) BE [eV] A [%]	O(2) BE [eV] A [%]	O(3) BE [eV] A [%]	N6 BE [eV] A [%]	N5 BE [eV] A [%]	NQ BE [eV] A [%]	N-X BE [eV] A [%]	II(1) BE [eV] A [%]	II(2) BE [eV] A [%]	II(3) BE [eV] A [%]	Shake-up BE [eV] A [%]	II(1) BE [eV] A [%]	II(2) BE [eV] A [%]	Shake-up BE [eV] A [%]
PNiD800	93.6	3.6	2.5	0.3	-	284.4 (66.4)	285.5 (30.0)	287.6 (3.6)	-	-	530.6 (26.9)	531.9 (44.3)	533.3 (28.8)	398.4 (39.2)	399.7 (28.3)	401.0 (32.4)	-	852.7 (9.2)	854.2 (43.8)	855.4 (47.0)	-	-	-	-
PNiD900	94.8	2.1	2.9	0.2	-	284.5 (69.3)	285.5 (28.4)	287.6 (2.3)	-	-	530.7 (23.9)	532.2 (55.1)	533.8 (21.0)	398.4 (48.6)	-	400.8 (51.4)	-	852.7 (5.4)	854.2 (64.2)	855.7 (30.4)	-	-	-	-
PNiH900	94.6	1.3	3.8	0.3	-	284.5 (55.0)	285.6 (25.0)	287.6 (15.3)	289.2 (1.2)	290.7 (3.5)	531.1 (63.9)	533.6 (32.1)	535.5 (4.0)	398.2 (38.2)	399.8 (18.8)	400.9 (30.3)	402.4 (12.6)	-	854.2 (21.5)	855.9 (9.5)	862.4 (27.2)	-	-	-
PFeD800	93.8	3.0	3.1	-	0.1	284.5 (66.1)	285.5 (28.3)	287.6 (4.5)	289.2 (1.0)	-	530.3 (18.7)	531.6 (48.9)	533.1 (32.4)	398.3 (44.2)	400.3 (32.7)	401.1 (23.0)	-	-	-	-	-	-	-	-
PFeD900	95.8	1.7	2.4	-	0.1	284.5 (70.5)	285.5 (27.5)	289.2 (1.0)	-	-	530.3 (19.0)	531.8 (57.6)	533.3 (23.3)	398.4 (31.8)	399.8 (11.2)	401.0 (57.0)	-	-	-	-	-	-	-	-
PFeH900	93.2	2.0	4.4	-	0.4	284.5 (63.9)	285.9 (23.8)	287.6 (9.0)	289.2 (0.5)	290.7 (2.9)	531.0 (60.2)	533.7 (36.3)	535.6 (3.5)	398.2 (31.5)	399.8 (19.6)	400.8 (26.5)	402.0 (22.5)	-	-	-	-	710.2 (33.8)	711.8 (54.9)	714.8 (11.4)

*Assignment of the peaks: CI: hydrocarbons, aromatics and aliphatics; CII: Csp^3 and C-O single bonds associated with ethers, phenols and anhydrides; CIII: C=O double bonds in carbonyls and quinones; CIV: C-O single bonds in carboxyls; CV: plasmon losses or shake-up π-π satellites. O(1): O–Metal bonds in metal oxides; O(2): C=O double bonds in quinone-type groups, carbonyls and carboxylic acids; O(3): –OH bonds in phenols, C–O–C ether groups and C=O bonds in ester and anhydride groups. N(6): pyridinic nitrogen; N(5): pyrrolic nitrogen; N(Q): quaternary nitrogen; N(X): nitrogen oxides. $Ni2p^{3/2}$ II(1): Ni^0; $Ni2p^{3/2}$ II(2): NiO; $Ni2p^{3/2}$ III(3): Ni-C complexes. $Fe2p^{3/2}$ II(1) and II(2): Fe(III). BE (eV) and A (%) stand for binding energy and relative contribution based on peak areas, respectively.